Pergamon

Int. J. Heat Mass Transfer. Vol. 40, No. 2, pp. 447–459, 1997

0017–9310/97 $15.00+0.00

PII: S0017–9310(96)00072–5

The nonlinear Czochralski growing process of crystals with variable thermal properties

SENPUU LIN

Department of Mechanical Engineering, National Lien-Ho College of Technology and Commerce, Miao-Li, Taiwan 36012, Republic of China

and

CHI-CHUAN HWANG† and HONG-YU LAY

Department of Mechanical Engineering, Chung Yuan University, Chung Li, Taiwan 32023, Republic of China

(*Received* 16 *May* 1995 *and in final form* 30 *January* 1996)

Abstract—The nonlinear dynamic process of Czochralski crystal growth with variable thermal properties is studied by the perturbation method. After evaluating the order of magnitude of these thermal properties, it is found that the temperature-dependent thermal conductivity is the dominant parameter in this problem. Comparing the results with that of the constant thermal conductivity model, we find that at the initial transient stage the difference between these models is insignificant, while the model difference is enlarged gradually, and at the final steady stage the model difference is the largest. Moreover, during the process, the higher the temperature difference between the crystal melting point and the surroundings is, the larger is the model difference. Finally, to avoid the computational burden, in this article, an optimal constant value of thermal conductivity is recommended. Copyright © 1996 Elsevier Science Ltd.

1. INTRODUCTION

Recently, Hwang *et al.* [1] have studied the nonlinear dynamic process of Czochralski (CZ) crystal growth with constant radius by the perturbation method and found that for growth under constant bulk melt temperature (pull rate), the pull rate (bulk melt temperature) would increase with increasing ambient Biot number for convective heat transfer from melt. Also, it was shown that the pull rate must not exceed the maximum value, otherwise the process will break down if the melt could not be supercooled (cf. ref. [1]).

However, conclusions based on the theoretical description of any physical process are strongly dependent on a knowledge of the numerical values of the various parameters appearing in the formalism. Hence, it is imperative to critically survey the available information concerning the parameters relevant to a realistic modeling and analysis of CZ crystal growth [2]. When temperature variations are large or the thermal properties vary rapidly with temperature, a valid description of the heat-conduction problem must take into account the variation of the transport coefficients with temperature. Then the differential equation of energy transport becomes nonlinear. Because the nonlinearity of energy balance equation and the time-dependent boundary conditions in CZ process eliminate the possibility of finding an exact analytical solution, the finite-element (or difference) solutions of the nonlinear CZ crystal growth model were used to predict crystal temperature distributions, pull rate and the thermal stresses by many authors [3–9]. Hwang *et al.* [10, 11] successfully adopted the perturbation method to investigate the effects of wall conduction and interface thermal resistance on the phase-change problem, as well as analysed unsteady thermoelastic dislocation generation during Czochralski crystal growth. Aziz and Lunardini [12] reviewed perturbation techniques in phase change heat transfer. The variable-property Stefan problem in which the thermal conductivity and specific heat of the solid phase are temperature-dependent has been studied by Aziz [13] and Pedroso and Domoto [14] using a regular perturbation method.

In the present work, the perturbation technique is extended to the nonlinear dynamic model of CZ crystal growth to examine the effect of variable thermal properties on the process. A comparison is made between the present results and the results of the temperature-independent thermal properties model to show the effect of variable thermal properties on the temperature distributions and the pull rate of the crystal as well as the temperature of the bulk melt during the process.

† Author to whom correspondence should be addressed.

NOMENCLATURE

c	specific heat capacity of crystal
c^*	dimensionless specific heat capacity of crystal
c_a	specific heat capacity of crystal at the ambient temperature
h_l	convective heat transfer coefficient for top surface of crystal
h_m	convective heat transfer coefficient for melt
h_r	convective heat transfer coefficient for cylindrical surface of crystal
k	thermal conductivity of crystal
k^*	dimensionless thermal conductivity of crystal
k_a	thermal conductivity of crystal at the ambient temperature
k_f	thermal conductivity of crystal at the melting temperature
l	heat of fusion
p	parameter in dimensionless pull rate εp, $dS/d\tau$
p_i	coefficient of ε^i in equation (24)
r	radial position
r_0	crystal radius
S	dimensionless crystal length, s/r_0
s	crystal length
S_0	dimensionless initial crystal length, s_0/r_0
s_0	initial crystal length
T	temperature of crystal
T_a	ambient temperature
T_f	solidification temperature of crystal
T_m	bulk melt temperature
t	time
v	crystal pull rate, ds/dt
z	axial position.

Greek symbols

α_i	parameter of specific heat in equation (9)
α_i^*	dimensionless parameter of specific heat in equation (22)
β_i	parameter of thermal conductivity in equation (8)
β_i^*	dimensionless parameter of thermal conductivity in equation (21)
β_l	Biot number of the top surface, $h_l r_0/k_a$
β_m	Biot number of the melt, $h_m r_0/k_a$
β_r	Biot number of the cylindrical surface, $h_r r_0/k_a$
γ_i	parameter of density in equation (10)
δ	dimensionless bulk melt temperature, $(T_m-T_a)/(T_f-T_a)$
ε	Stefan number, $c_a(T_f-T_a)/l$
εp	dimensionless pull rate, $\rho_a c_a v r_0/k_a$
θ	dimenionless temperature, $(T-T_a)/(T_f-T_a)$
ρ	density of crystal
ρ^*	dimensionless density of crystal
ρ_a	density of crystal at the ambient temperature
τ	dimensionless time, $\varepsilon k_a t/\rho_a c_a r_0^2$
ψ	dimensionless axial position, z/r_0.

2. ANALYSIS

The plant configuration of a CZ process is shown in Fig. 1. The following assumptions are introduced [1,7]:

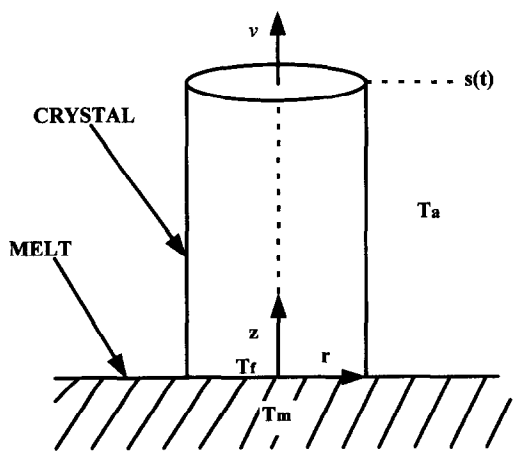

Fig. 1. Schematic model for CZ crystal growth process.

(1) Growth of constant radius crystal is desired by perfect control of the crystal pull rate, v and/or bulk melt temperature, T_m.
(2) Radial temperature variations are small and can be described by the "fin-approximation".
(3) Axial symmetry in the crystal.
(4) Thermal properties of crystal (density, ρ; specific heat, c; thermal conductivity, k) are temperature-dependent, but the other properties (including heat transfer coefficient h_r, h_l, h_m for cylindrical surface, top surface and the melt, respectively) are assumed to be temperature-independent.
(5) Heat transfer between the crystal and the surroundings in governed by Newton's law of cooling to an ambient temperature which is independent of position and time.
(6) Heat transfer between the crystal and the melt is governed by Newton's law of cooling to a bulk melt temperature T_m which is independent of position.
(7) The crystal–melt interface at the solidification temperature T_f is planar and fixed at the origin of the coordinate system.
(8) The crystal initially has some small length s_0.

In the coordinate system with the origin at the stationary crystal–melt interface, the nonlinear dynamic energy transport describing the CZ process can be written in the following form

$$\rho(T)c(T)\left(\frac{\partial T}{\partial t}+v\frac{\partial T}{\partial z}\right)=\frac{\partial}{\partial z}\left[k(T)\frac{\partial T}{\partial z}\right]-2\frac{h_r}{r_0}(T-T_a)\quad 0\leqslant z\leqslant s(t) \tag{1}$$

$$T(z,t)=T_f \quad \text{at } t=0 \tag{2}$$

$$T(z,t)=T_f \quad \text{at } z=0 \tag{3}$$

$$k(T)\frac{\partial T}{\partial z}+h_l(T-T_a)=0 \quad \text{at } z=s(t) \tag{4}$$

$$\rho(T)l\frac{ds}{dt}=-\left[k(T)\frac{\partial T}{\partial z}+h_m(T_m-T_f)\right] \quad \text{at } z=0 \tag{5}$$

$$s=s_0 \quad \text{at } t=0 \tag{6}$$

$$v=\frac{ds}{dt} \tag{7}$$

and

$$k(T)=k_a[1+\beta_1(T-T_a)+\beta_2(T-T_a)^2+\beta_3(T-T_a)^3+\cdots] \tag{8}$$

$$c(T)=c_a[1+\alpha_1(T-T_a)+\alpha_2(T-T_a)^2+\alpha_3(T-T_a)^3+\cdots] \tag{9}$$

$$\rho(T)=\rho_a[1+\gamma_1(T-T_a)+\gamma_2(T-T_a)^2+\gamma_3(T-T_a)^3+\cdots]. \tag{10}$$

Following our previous work [1], we choose the Stefan number ε, which signifies the importance of sensible heat to the latent heat, as a small perturbation parameter. After defining the dimensionless variables of temperature θ, axial position ψ, pull rate εp, time τ, crystal length S, bulk melt temperature δ and Stefan number ε as:

$$\theta=\frac{T-T_a}{T_f-T_a}\quad \psi=\frac{z}{r_0}\quad \varepsilon p=\frac{\rho_a c_a v r_0}{k_a}\quad \tau=\frac{\varepsilon k_a t}{\rho_a c_a r_0^2}$$

$$S=\frac{s}{r_0}\quad \delta=\frac{T_m-T_a}{T_f-T_a}\quad \varepsilon=\frac{c_a(T_f-T_a)}{l}$$

where T is the temperature of crystal, T_a is the ambient temperature, z is axial position, t is time, ρ_a is the density of crystal at T_a, c_a is the specific heat capacity of crystal at T_a, k_a is the thermal conductivity of crystal at T_a, l is the specific enthalpy of solidification, s is crystal length and r_0 is crystal radius, equations (1)–(10) will become

$$\rho^*(\theta)c^*(\theta)\varepsilon p\left(\frac{\partial\theta}{\partial S}+\frac{\partial\theta}{\partial\psi}\right)=\frac{\partial}{\partial\psi}\left[k^*(\theta)\frac{\partial\theta}{\partial\psi}\right]-2\beta_r\theta\quad 0\leqslant\psi\leqslant S(\tau) \tag{11}$$

$$\theta(\psi,\tau)=1 \quad \text{at } \tau=0 \tag{12}$$

$$\theta(\psi,\tau)=1 \quad \text{at } \psi=0 \tag{13}$$

$$k^*(\theta)\frac{\partial\theta}{\partial\psi}+\beta_l\theta=0 \quad \text{at } \psi=S(\tau) \tag{14}$$

$$\rho^*(\theta)p=-\left[k^*(\theta)\frac{\partial\theta}{\partial\psi}+\beta_m(\delta-1)\right] \quad \text{at } \psi=0 \tag{15}$$

$$S(\tau)=S_0 \quad \text{at } \tau=0 \tag{16}$$

$$p=\frac{dS}{d\tau} \tag{17}$$

$$k^*(\theta)=1+\beta_1(T_f-T_a)\theta+\beta_2(T_f-T_a)^2\theta^2+\beta_3(T_f-T_a)^3\theta^3+\cdots \tag{18}$$

$$c^*(\theta)=1+\alpha_1(T_f-T_a)\theta+\alpha_2(T_f-T_a)^2\theta^2+\alpha_3(T_f-T_a)^3\theta^3+\cdots \tag{19}$$

$$\rho^*(\theta)=1+\gamma_1(T_f-T_a)\theta+\gamma_2(T_f-T_a)^2\theta^2+\gamma_3(T_f-T_a)^3\theta^3+\cdots \tag{20}$$

In the above system, equation (11) is the energy equation, equation (12) and equation (16) are initial conditions, equation (13) and equation (14) are boundary conditions and equation (15) is the energy balance at the crystal–melt interface, where $\beta_r=h_r r_0/k_a$ and $\beta_l=h_l r_0/k_a$ are the ambient Biot numbers for convective heat transfer from cylindrical surface and top surface, $\beta_m=h_m r_0/k_a$ is the melt Biot number for convective heat transfer from melt, $S_0=s_0/r_0$ is the dimensionless initial crystal length.

The thermophysical properties in present numerical calculations to model GaAs and Si systems are listed in Table 1 [2, 8], where the temperature dependency of the thermal conductivity, the specific heat as well as the density of the crystal are taken into account.

In practice, the magnitude of thermal property parameters such as $\alpha_1(T_f-T_a)$, $\alpha_2(T_f-T_a)^2$, $\beta_1(T_f-T_a)$, $\beta_2(T_f-T_a)^2$, $\beta_3(T_f-T_a)^3$ in equations (18)–(20) is small. To be appropriate for the perturbation analysis, the evaluations of these thermal property parameters for our selected reference cases (I), (II), (III) and (IV) are listed in Table 2. For simplicity, we only choose four cases to study and the order of magnitude of these thermal properties in those cases are adjusted as

$$k^*(\theta)=\begin{cases}1+\varepsilon\beta_1^*\theta+\varepsilon^2\beta_2^*\theta^2 \\ \quad \text{for (I) GaAs, } T_f-T_a=200\,\text{K} \\ 1+\varepsilon\beta_1^*\theta+\varepsilon^2\beta_2^*\theta^2+\varepsilon^2\beta_3^*\theta^3 \\ \quad \text{for (II) GaAs, } T_f-T_a=400\,\text{K} \\ 1+\varepsilon^2\beta_1^*\theta+\varepsilon^2\beta_2^*\theta^2 \\ \quad \text{for (III) Si, } T_f-T_a=400\,\text{K} \\ 1+\varepsilon^2\beta_1^*\theta+\varepsilon^2\beta_2^*\theta^2 \\ \quad \text{for (IV) Si, } T_f-T_a=500\,\text{K}\end{cases} \tag{21}$$

Table 1. Thermophysical properties of GaAs and Si crystal [2, 3, 6, 7]

Property	GaAs	Si
Heat of fusion, I [J g^{-1}]	726	1105.3
Melting temperature of crystal, T_f [K]	1511	1685.15
Thermal conductivity, k [W cm^{-1} K^{-1}]	$208T^{-1.09}$	$529.382/T$ -376.764×10^{-3} $+169.524\times10^{-6}T$
Specific heat, c [J g^{-1} K^{-1}]	$0.302+8.1\times10^{-5}T$	$-1.3298\times10^{4}/T^{2}$ $+8.1711\times10^{-1}$ $+169.524\times10^{-6}T$
Density, ρ [g cm^{-3}]	$5.32-9.91\times10^{-5}T$	$2.3388-2.9508\times10^{-5}T$

Table 2. The evaluations of thermal property parameters in reference cases for 2nd order perturbation analysis in modeling GaAs and Si systems [2, 3, 6, 7]

Property	CASE I GaAs	CASE II GaAs	CASE III Si	CASE IV Si
T_f-T_a	200 K	400 K	400 K	500 K
$h'(T_a)$	0.0021†	0.0019†	—	—
I	4 cm†	4 cm†	—	—
Perturbation quantity, ε	0.11245	0.21597	0.35558	0.43774
$\alpha_1(T_f-T_a)$	$O(\varepsilon^2)$	$O(\varepsilon^2)$	$O(\varepsilon^3)$	$O(\varepsilon^4)$
$\alpha_2(T_f-T_a)^2$	—	—	$O(\varepsilon^6)$	$O(\varepsilon^5)$
$\gamma_1(T_f-T_a)$	$O(\varepsilon^3)$	$O(\varepsilon^4)$	$O(\varepsilon^6)$	$O(\varepsilon^5)$
$\beta_1(T_f-T_a)$	$O(\varepsilon)$	$O(\varepsilon)$	$O(\varepsilon^2)$	$O(\varepsilon^2)$
$\beta_2(T_f-T_a)^2$	$O(\varepsilon^2)$	$O(\varepsilon^2)$	$O(\varepsilon^2)$	$O(\varepsilon^2)$
$\beta_3(T_f-T_a)^3$	$O(\varepsilon^3)$	$O(\varepsilon^2)$	$O(\varepsilon^3)$	$O(\varepsilon^3)$
$\beta_4(T_f-T_a)^4$	$O(\varepsilon_4)$	$O(\varepsilon^3)$	$O(\varepsilon^5)$	$O(\varepsilon^4)$
$\eta_1(T_f-T_a)$	$O(\varepsilon)$	$O(\varepsilon)$	$O(\varepsilon)$	$O(\varepsilon)$
$\eta_2(T_f-T_a)^2$	$O(\varepsilon^2)$	$O(\varepsilon)$	$O(\varepsilon^3)$	$O(\varepsilon^3)$
$\eta_3(T_f-T_a)^3$	$O(\varepsilon^3)$	$O(\varepsilon^3)$	$O(\varepsilon^5)$	$O(\varepsilon^4)$
$c^*(\theta)$	$1+\varepsilon^2\alpha_1^*\theta$	$1+\varepsilon^2\alpha_1^*\theta$	1	1
$\rho^*(\theta)$	1	1	1	1
$k^*(\theta)$	$1+\varepsilon\beta_1^*\theta+\varepsilon^2\beta_2^*\theta^2$	$1+\varepsilon\beta_1^*\theta+\varepsilon^2\beta_2^*\theta^2+\varepsilon^2\beta_3^*\theta^3$	$1+\varepsilon^2\beta_1^*\theta+\varepsilon^2\beta_2^*\theta^2$	$1+\varepsilon^2\beta_1^*\theta+\varepsilon^2\beta_2^*$
$h^*(\theta)$	$1+\varepsilon\eta_1^*\theta+\varepsilon^2\eta_2^*\theta^2$	$1+\varepsilon\eta_1^*\theta+\varepsilon\eta_2^*\theta^2$	$1+\varepsilon\eta_1^*\theta$	$1+\varepsilon\eta_1^*\theta$
α_1^*	3.138615	8.265496	—	—
β_1^*	−1.4876	−1.81708	−1.88798	−1.99809
β_2^*	2.09645	3.16545	1.24734	1.53208
β_3^*	—	−1.17387	—	—
η_1^*	2.85085	3.43596	1.22109	1.36410
η_2^*	3.50079	1.10536	—	—

† cf. Table 2 in ref. [2]; for $A_{(g)}$.

$$c^*(\theta)=\begin{cases}1+\varepsilon^2\alpha_1^*\theta & \text{for (I), (II)}\\ 1 & \text{for (III), (IV)}\end{cases} \tag{22}$$

$$\rho^*(\theta)=1 \quad \text{for (I), (II), (III), (IV).} \tag{23}$$

From above expressions, the temperature-dependent thermal conductivity is the dominant parameter in this problem.

According to the analysis of the previous paper [1], for constant radius crystal growth, the pull rate and/or the bulk melt temperature are usually varied. The effects of temperature-dependent thermal conductivity on both the case of varying pull rate under fixed bulk melt temperature and the case of varying bulk melt temperature under constant pull rate are investigated.

2.1. *Growth under fixed bulk melt temperature δ and varying pull rate εp*

To determine the solutions of crystal temperature distribution and pull rate, let us express the perturbation solutions as

$$\theta=\theta_0+\varepsilon\theta_1+\varepsilon^2\theta_2+\cdots$$

$$p=p_0+\varepsilon p_1+\varepsilon^2 p_2+\cdots \tag{24}$$

The solutions to the system are

$$\theta_0=\frac{Je^{A\psi}+Ie^{-A\psi}}{L} \tag{25}$$

$$\theta_1 = (C_1 + C_2\psi)e^{A\psi} + (C_3 + C_4\psi)e^{-A\psi} + C_5 e^{2A\psi} + C_6 e^{-2A\psi} \quad (26)$$

$$\theta_2 = (E_1 + E_2\psi + E_3\psi^2)e^{A\psi} + (E_4 + E_5\psi + E_6\psi^2)e^{-A\psi} + (E_7 + E_8\psi)e^{2A\psi} + (E_9 + E_{10}\psi)e^{-2A\psi} + E_{11}e^{3A\psi} + E_{12}e^{-3A\psi} + E_{13}e^{4A\psi} + E_{14}e^{-3A\psi} \quad (27)$$

and

$$p_0 = \frac{A(I-J)}{L} - \beta_m(\delta - 1) \quad (28)$$

$$p_1 = -(C_2 + C_4) - A(C_1 - C_3) - 2A(C_5 - C_6) + F \quad (29)$$

$$p_2 = -(E_2 + E_5 + E_8 + E_{10}) - A(E_1 - E_4) - 2A(E_7 - E_9) - 3A(E_{11} - E_{12}) - 4A(E_{13} - E_{14}) + G \quad (30)$$

here A, I, J, L, $C_1, \ldots, C_6$, $E_1, \ldots, E_{14}$, F and G are derived in the Appendix.

Assuming that the melt can not be supercooled (i.e. $\delta \not< 1$) and is continuously maintained at the melting temperature ($\delta = 1$, the minimum value) then the pull rate will be the maximum value of the process and can be defined as the maximum pull rate $(\varepsilon p)_{max}$ (cf. Fig. 2 in ref. [1]). It is found to be

$$(\varepsilon p)_{max} = \varepsilon(p_0 + \varepsilon p_1 + \varepsilon^2 p_2)$$

from the above perturbation solutions (28)–(30) and equation (24) as δ is equal to 1. So, the crystal pull rate during the process can not exceed the maximum pull rate at the instant otherwise solidification does not occur and single crystal is not grown.

2.2. *Growth under fixed pull rate* εp *and varying melt temperature* δ

The perturbation solutions for the temperature θ and bulk melt temperature δ up to the second-order can be found as

$$\theta = \theta_0 + \varepsilon\theta_1 + \varepsilon^2\theta_2 \quad (31)$$

where

$$\theta_0 = \frac{Je^{A\psi} + Ie^{-A\psi}}{L} \quad (32)$$

$$\theta_1 = (C_1 + C_2\psi)e^{A\psi} + (C_3 + C_4\psi)e^{-A\psi} + C_5 e^{2A\psi} - C_6 e^{-2A\psi} \quad (33)$$

$$\theta_2 = (E_1 + E_2\psi + E_3\psi^2)e^{A\psi} + (E_4 + E_5\psi + E_6\psi^2)e^{-A\psi} + (E_7 + E_8\psi)e^{2A\psi} + (E_9 + E_{10}\psi)e^{-2A\psi} + E_{11}e^{3A\psi} + E_{12}e^{-3A\psi} + E_{13}e^{4A\psi} + E_{14}e^{-4A\psi} \quad (34)$$

and

$$\delta = \delta_0 + \varepsilon\delta_1 + \varepsilon^2\delta_2. \quad (35)$$

$$\delta_0 = 1 - \frac{p}{\beta_m} - \frac{A(I-J)}{L\beta_m} \quad (36)$$

$$\delta_1 = -\frac{1}{\beta_m}[(C_2 + C_4) + A(C_1 - C_3) + 2A(C_5 - C_6) + F] \quad (37)$$

$$\delta_2 = -\frac{1}{\beta_m}[(E_2 + E_5 + E_8 + E_{10}) + A(E_1 - E_4) + 2A(E_7 - E_9) + 3A(E_{11} - E_{12}) + 4A(E_{13} - E_{14}) + G]. \quad (38)$$

here A, I, J, L, $C_1, \ldots, C_6$, $E_1, \ldots, E_{14}$, F and G are the same as equations (A16)–(A57) (cf. Appendix) but replacing p_0 and p_1 with p and 0, respectively.

It is noted that the crystal length S now is expressed as $S = \varepsilon p\tau + S_0$. If it is assumed that the melt cannot be supercooled initially, then the maximum pull rate $(\varepsilon p)_{max}$ is attained when $\delta(\tau = 0) = 1$. Here, the $(\varepsilon p)_{max}$ (constant) can be derived from equations (35)–(38) when $\tau = 0$ and $\delta = 1$. So, the constant pull rate must be controlled below $(\varepsilon p)_{max}$ otherwise single crystal is not grown and the constant radius cystal growth under fixed pull rate can be obtained by increasing melt temperature δ [1].

3. RESULTS AND DISCUSSION

For comparison between our previous first-order [1], the present second-order perturbation solutions and the finite-difference results of Venerus [7], Fig. 2 shows the evolution of pull rate εp for different Stefan numbers with temperature-independent thermal properties, $\delta = 1.0$, $\beta_l = 0.1 = \beta_s$, $\beta_m = 1.0$ and $S_0 = 0.1$. Improving the preceding first-order perturbation solutions, the results of the second-order perturbation analysis are in conformity with the work of Venerus [7] and the accuracy of present results is

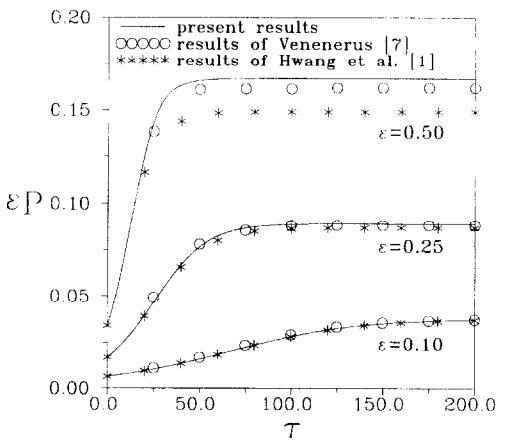

Fig. 2. The evolution of crystal pull rate for three different Stefan numbers with $\delta = 1.05$, $\beta_r = 0.1 = \beta_l$, $\beta_m = 1.0$ and $S_0 = 0.1$. Comparison is made between our present results and the previous results.

more than that of the first-order solutions at least in the case of $\varepsilon = 0.5$. Also, from this figure, two distinct stages are clearly seen for all the curves. In the initial stage, referred as the transient stage, the εp increases with time. Finally, the εp is independent of time and will be referred to as steady state. This can be explained from the energy balance equation (15) for the crystal–melt interface under $k^*(\theta) = 1 = c^*(\theta) = \rho^*(\theta)$. In the left-hand side of the equation, the term p times Stefan number ε is the pull rate of crystal, εp, that is proportional to the ratio of sensible to latent heat of phase change. In the right-hand side, the terms $\partial\theta/\partial\psi$ and $\beta_m(\delta - 1)$ represent energy transport from interface into crystal and from melt into interface, respectively, and the minus sign is included to ensure that the heat flow is in the positive ψ direction. The $\partial\theta/\partial\psi$ is calculated from equations (11)–(14) and has the relations with the ambient Biot numbers. By the definition of the ambient Biot number, the rate of eternal energy transport of crystal is increased, results in a decrease in $\partial\theta/\partial\psi$. During the transient stage, an increase in crystal length allows for more energy to be released at the crystal–melt interface, which increases the rate of external energy transport of crystal so that $\partial\theta/\partial\psi$ decreases, and hence, with the minus sign, an increase in εp. Afterwards, during the steady stage, increasing crystal length no longer affects the external energy transport so that the εp becomes steady [1, 7].

The thermophysical properties in present numerical calculations to model GaAs and Si systems are listed in Table 1 [2, 8], where the temperature dependency of the thermal conductivity of crystal and the specific heat of crystal as well as the density of crystal is taken into account. For simplicity, we choose four cases listed in Table 2 to study. After evaluating the order of magnitude of these thermal properties listed in Table 2, it is found that only the temperature-dependent thermal conductivity is important in this problem.

A constant radius crystal is grown by perfect control of the crystal pull rate, εp and/or bulk melt temperature δ [1]. The following two types of results are discussed to indicate the effect of the variable thermal conductivity on the process.

3.1. *Growth under fixed melt temperature and varying pull rate*

Figures 3(a) and (b) show the effects of the temperature-dependent thermal conductivity k (temperature-dependent k model) on the evolution of pull rate εp in GaAs crystal growth with constant crystal radius, $\beta_m = 1.0$, $\beta_r = 0.1 = \beta_l$, $\delta = 1.0$, $S_0 = 0.1$ for $T_f - T_a = 200$K and $T_f - T_a = 400$K, respectively. As the temperature dependency of the thermal conductivity of crystal is not taken into account, both the model of constant thermal conductivity at the ambient temperature T_a ($k^*(\theta = 0)$, constant k_a model) and the model of constant thermal conductivity at the solidification temperature T_f of crystal ($k^*(\theta = 1)$,

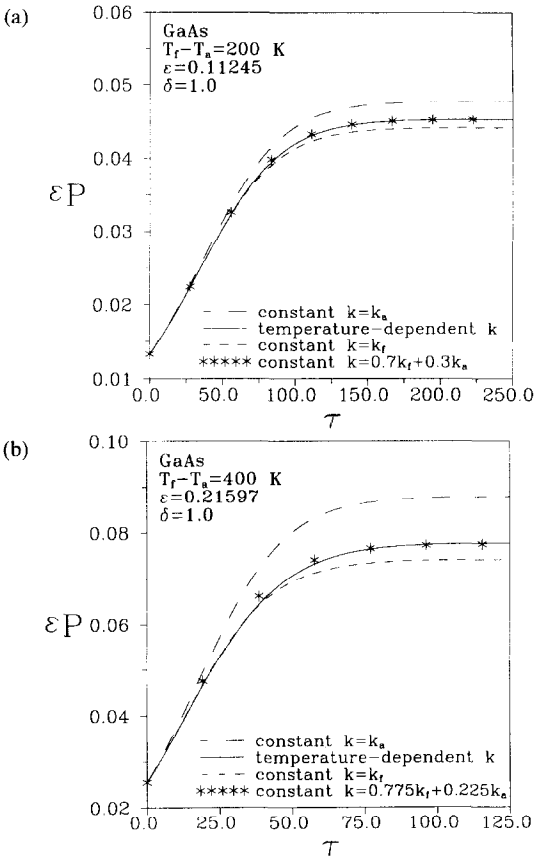

Fig. 3. Effect of temperature-dependent thermal conductivity on the evolution of crystal pull rate in GaAs crystal growth with constant crystal radius, $\beta_m = 1.0$, $\beta_r = 0.1 = \beta_l$, $S_0 = 0.1$, $\delta = 1.0$ for (a) $T_f - T_a = 200$K and (b) $T_f - T_a = 400$K, respectively.

constant k_f model) is considered. In Figs. 4(a) and (b) are also shown the effects of the temperature-dependent k on the evolution of εp in Si crystal growth with constant crystal radius, $\beta_m = 1.0$ $\beta_r = 0.1 = \beta_l$, $\delta = 1.0$, $S_0 = 0.1$ for $T_f - T_a = 400$K and $T_f - T_a = 500$K, respectively. From these figures, two distinct transient and steady stages are also seen clearly. If the bulk melt is superheated ($\delta > 1$), increasing β_m results in a decrease in εp (cf. Fig. 2 in ref. [1]). When the bulk melt is always at the melting temperature ($\delta = 1.0$), the pull rate is found to be the maximum value of the process and independent of β_m if it is assumed that the melt can not be supercooled. Crystal growth control is not admissible during this process as εp exceeds the maximum pull rate (cf. Fig. 2 in ref. [1]). Apparently, the allowable maximum pull rate (as $\delta = 1$) for crystal growth is affected by the temperature-dependent k. For example, the allowable maximum pull rate at the steady stage for GaAs with $T_f - T_a = 400$K in the temperature-dependent k model is about 13% less than that in the constant k_a model, but about 5% greater than that in the constant k_f model, while, at the initial transient stage, the difference between these models is not significant. Gradually, the effect of variable k on the allowable maximum

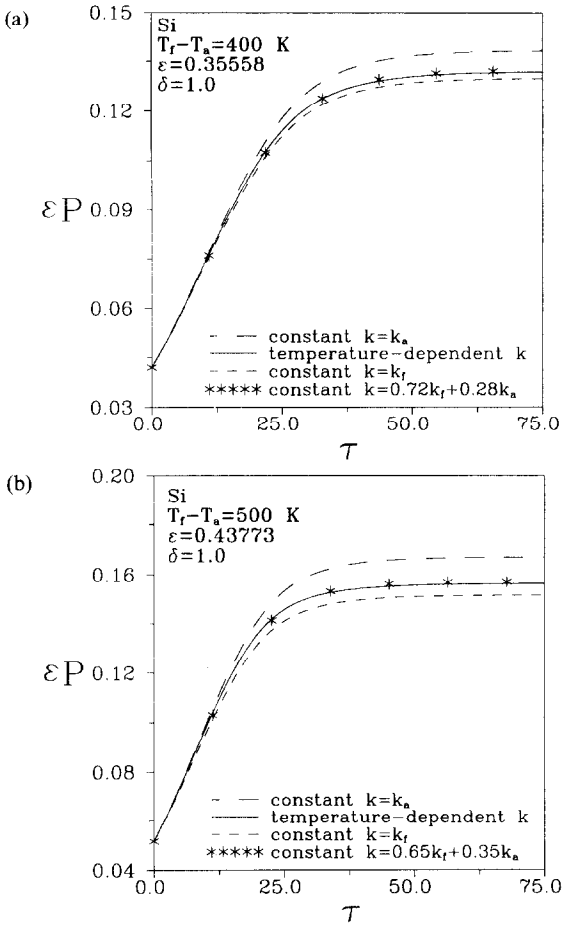

Fig. 4. Effect of temperature-dependent thermal conductivity on the evolution of crystal pull rate in Si crystal growth with constant crystal radius, $\beta_m = 1.0$, $\beta_r = 0.1 = \beta_l$, $S_0 = 0.1$, $\delta = 1.0$ for (a) $T_f - T_a = 400$K and (b) $T_f - T_a = 500$K, respectively.

pull rate during the process is enlarged, and the difference of the allowable maximum pull rate at the steady stage between these models is the largest. The above behaviors can be also explained from the energy balance equation (15) for the crystal–melt interface. In the left-hand side of the equation ($\rho^*(\theta) = 1.$), the term p times Stefan number ε is the pull rate of crystal, εp, that is proportional to the ratio of sensible to latent heat of phase change. In the right-hand side, the terms $k^*(\theta)\partial\theta/\partial\psi$ and $\beta_m(\delta - 1)$ represent energy transport from interface into crystal and from melt into interface, respectively, and the minus sign is included to ensure that the heat flow is in the positive ψ direction. At the initial transient stage, the time scale associated with heat transfer is much greater than the time scale for geometry changes in crystal length, so that the $\partial\theta/\partial\psi$ in these models is almost the same. However, the term $k^*(\theta)$ in the constant k_a model is the highest among these three models, that in the temperature-dependent k model is the second, and that in the constant k_f model is the lowest. Then, the $k^*(\theta)\partial\theta/\partial\psi$ in the constant k_a model is the largest, that in the temperature-dependent k model is second and that in the constant k_f model is the smallest. And hence, with the minus sign, the increment in pull rate εp in the constant k_a model is the largest, that in the temperature-dependent k model is the second, and that in the constant k_f model is the smallest. Afterwards, at the steady stage, the time scale associated with heat transfer is much smaller than the time scale for geometry changes in crystal length. There is enough time for energy transport in the crystal so that the difference in the $\partial\theta/\partial\psi$ between the models is very small, then as mentioned previously, the pull rate in the constant k_a model is the highest, that in the temperature-dependent k model is the second and that in the constant k_f model is the lowest.

Moreover, from these figures, it is found that the higher the temperature difference between the crystal melting point and the surroundings ($T_f - T_a$) is, the larger is the difference of the allowable maximum pull rate between these models during the process. We can explain this result by the definition of Stefan number. As increasing ($T_f - T_a$) results in an increase in Stefan number ε, the ratio of heat which can be stored within the crystal to the heat released by solidification increases, and this leads to an increase in εp. Correspondingly, the difference of the allowable maximum pull rate between these models increases with increasing ($T_f - T_a$).

According to the above analysis, one can predict that the temperature gradients ($\partial\theta/\partial\psi$) in these models at the initial transient stage will be close to each other and at the steady state there is the same phenomenon. Evidence to support the above prediction is shown in Figs. 5 and 6. Figure 5 shows the effect of the temperature-dependent k on the temperature distributions of crystal θ in GaAs crystal growth with constant crystal radius, $\beta_m = 1.0$, $\beta_r = 0.1 = \beta_l$,

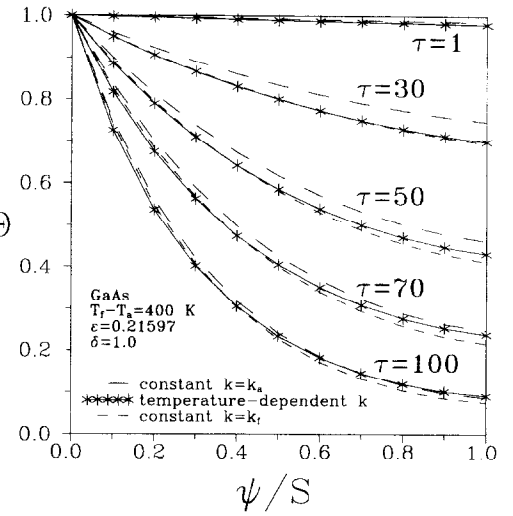

Fig. 5. Effect of temperature-dependent thermal conductivity on temperature distributions in axial position at different time, for in GaAs crystal growth with constant crystal radius, $\beta_m = 1.0$, $\beta_r = 0.1 = \beta_l$, $S_0 = 0.1$, $\delta = 1.0$ for $T_f - T_a = 400$K.

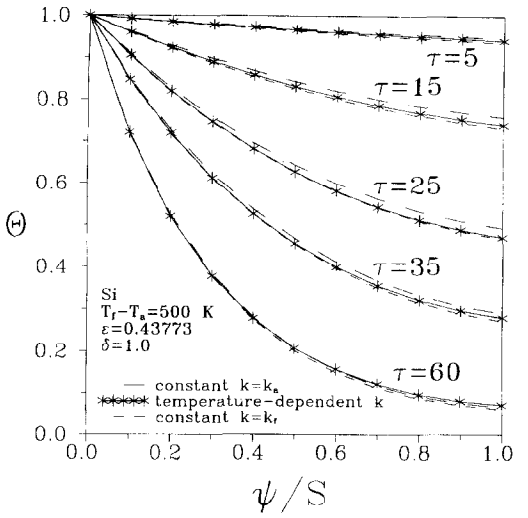

Fig. 6. Effect of temperature-dependent thermal conductivity on temperature distributions in axial position at different time, for in Si crystal growth with constant crystal radius, $\beta_m = 1.0, \beta_r = 0.1 = \beta_l, S_0 = 0.1, \delta = 1.0$ for $T_f - T_a = 500$K.

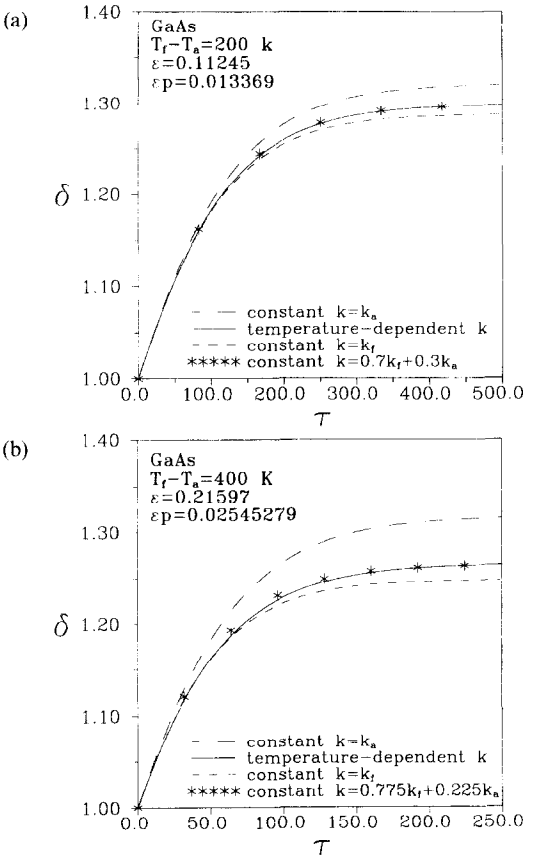

Fig. 7. Effect of temperature-dependent thermal conductivity on the evolution of bulk melt temperature in GaAs crystal growth with constant crystal radius, under fixed pull rate εp, $\beta_m = 1.0, \beta_r = 0.1 = \beta_l, S_0 = 0.1$, for (a) $T_f - T_a = 200$K and (b) $T_f - T_a = 400$K, respectively.

$\delta = 1.0$ and $T_f - T_a = 400$K. It is easy to see that the $\partial\theta/\partial\psi$ between these models is close to each other at the initial transient stage, and the difference of the $\partial\theta/\partial\psi$ between these models will enlarge with increasing time τ. However, after some interval, the increment in the difference of the $\partial\theta/\partial\psi$ between these models will stop and decrease with the increasing τ; afterwards, at the steady state the difference of the $\partial\theta/\partial\psi$ between these models is very small. For Si system, Fig. 6 shows the effect of the temperature-dependent k on the θ with constant crystal radius, $\beta_m = 1.0$, $\beta_r = 0.1 = \beta_l$, $\delta = 1.0$ and $T_f - T_a = 500$K. It is found that there are the same phenomena as in case of GaAs system.

Furthermore, we find that if the constant value of the combination of k_f and k_a; $0.7k_f + 0.3k_a$ for GaAs, $T_f - T_a = 200$K; $0.775k_f + 0.225k_a$ for GaAs, $T_f - T_a = 400$K; $0.72k_f + 0.28k_a$ for Si, $T_f - T_f - T_a = 400$ K; $0.65k_f + 0.35k_a$ for Si, $T_a = 500$K; is used to simulate the model of temperature-dependent thermal conductivity in the process, the model difference between the variable k and constant k will be insignificant.

3.2. *Growth under fixed pull rate and varying melt temperature*

Figures 7(a) and (b) show the effects of the temperature-dependent k on the evolution of bulk melt temperature δ in GaAs crystal growth with constant crystal radius, $\beta_m = 1.0$, $\beta_r = 0.1 = \beta_l$, $S_0 = 0.1$ for $T_f - T_a = 200$K and $T_f - T_a = 400$K, respectively. In Figs. 8(a) and (b) are also shown the effects of the temperature-dependent k on the evolution of δ in Si crystal growth with constant crystal radius, $\beta_m = 1.0$, $\beta_r = 0.1 = \beta_l$, $S_0 = 0.1$ for $T_f - T_a = 400$K and $T_f - T_a = 500$K, respectively. If the melt cannot be supercooled, one has to increase the δ for fixed εp growth with constant radius and, as the melt is initially at the melting temperature ($\delta = 1$), the value of εp is the maximum. The pull rate must be controlled below this maximum value during the process, otherwise the crystal is not grown [1]. In these figures, there are also two distinct stages. The first stage can be referred to as transient stage of δ and the second is the steady stage. It is found that there exists the effect of variable k on the evolution of δ. During the initial transient stage, the difference between these models is not significant; gradually, it will be enlarged during the process. Afterwards, at the final steady stage, the difference of the δ between these models is the largest. One also can explain this from the energy balance equation (15). At the initial transient stage, because, as mentioned previously, the $k^*(\theta)\partial\theta/\partial\psi$ in the constant k_a model is the largest, that in the temperature-dependent k model is second and that in the constant k_f model is the smallest, and hence, the increment in melt temperature in the constant k_a model is the largest, that in the temperature-dependent k model is second, and that in the constant k_f model is the smallest. At the steady stage, the difference in the $\partial\theta/\partial\psi$ between these models is very small, then the δ in the

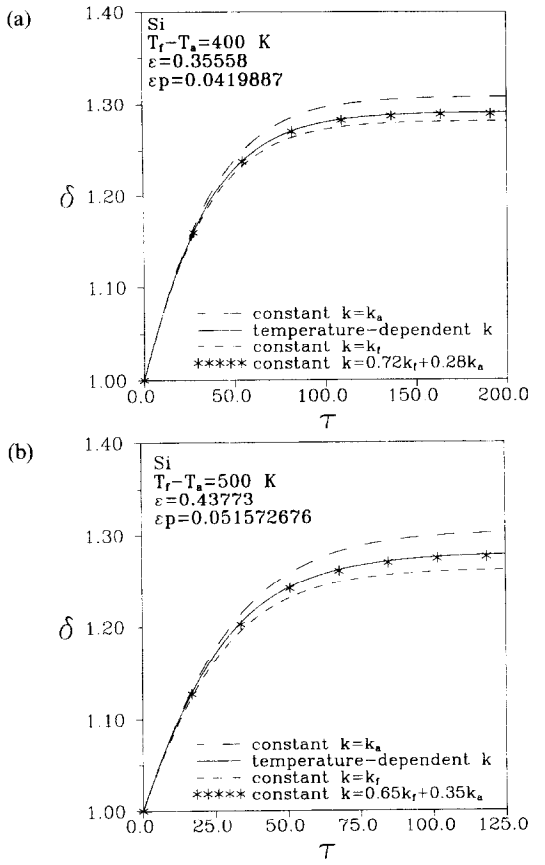

Fig. 8. Effect of temperature-dependent thermal conductivity on the evolution of bulk melt temperature in Si crystal growth with constant crystal radius, under fixed pull rate εp, $\beta_m = 1.0$, $\beta_r = 0.1 = \beta_l$, $S_0 = 0.1$, for (a) $T_f - T_a = 400$K and (b) $T_f - T_a$ 500K, respectively.

constant k_a model is the highest, that in the temperature-dependent k model is the second and that in the constant k_f model is the lowest. Also, it is found that the higher the difference between T_f and T_a is, the larger is the difference of the δ between these models.

In the real Cz furnace, the bulk melt temperature T_m is not necessarily uniform. Also, for high temperature materials, radiative heat transfer becomes important and temperature-dependent, Newton's law of cooling is not very useful for describing heat transfer at the melt–crystal interface as well as heat transfer between the crystal and the surroundings. The effect of the temperature-dependent heat transfer coefficient on the process will be considered in our further study.

4. CONCLUSIONS

To show the effects of temperature-dependent thermal properties on the nonlinear dynamic process of modeling GaAs and Si crystal growth. Conclusions are summarized as:

(1) After evaluating the order of magnitude of the thermal conductivity, specific heat and density of crystal, it is found that the temperature-dependent thermal conductivity is the dominant parameter in this problem.
(2) To grow a constant radius crystal under a fixed bulk melt temperature (pull rate), the pull rate (bulk melt temperature) will be affected by the variable thermal conductivity significantly.
(3) Comparing the results with that of the constant thermal conductivity model, we find that at the initial transient stage, the difference between these models is small, while, the effect of variable thermal conductivity on the pull rate (bulk melt temperature) during the process is enlarged, and at the final steady stage the difference of the pull rate (bulk melt temperature) between these models is the largest.
(4) During the process, the higher the temperature difference between the crystal melting point and the surroundings is, the larger is the model difference between the variable thermal conductivity model and the constant thermal conductivity model.
(5) To avoid the computational burden, in this article, a optimal constant value of thermal conductivity is recommended.

Acknowledgements—Support by the National Science Council of the Republic of China, through research grant no. NSC 83-0413-E-033-028, is gratefully acknowledged.

REFERENCES

1. C.-C. Hwang, K.-M. Chen and S. Lin, On the nonlinear dynamic process in Czochralski crystal growth, *J. Crystal Growth* **147**, 390–398 (1995).
2. A. S. Jordan, An evaluation of the thermal and elastic constants affecting GaAs crystal growth, *J. Crystal Growth* **49**, 631–642 (1980).
3. A. B. Crowley, Mathematical modelling of heat flow in Czochralski crystal pulling, *IMA J. Appl. Math.* **30**, 173–189 (1983).
4. J. J. Derby, L. J. Atherton, P. D. Thomas and R. A. Brown, Finite-element methods for analysis of the dynamics and control of Czochralski crystal growth, *J. Sci. Comput.* **2**, 297–343 (1987).
5. J. J. Derby and R. A. Brown, On the dynamics of Czochralski crystal growth, *J. Crystal Growth* **83**, 137–151 (1987).
6. H. Kopetsch, A numerical method for the time-dependent Stefan problem in Czochralski crystal growth, *J. Crystal Growth* **88**, 71–86 (1988).
7. D. C. Venerus, Analysis of finite length dynamics in Czochralski crystal growth, *J. Crystal Growth* **102**, 376–386 (1990).
8. A. Virzi, Computer modelling of heat transfer in Czochralski silicon growth, *J. Crystal Growth* **112**, 699–722 (1991).
9. D. E. Bornside, T. A. Kinney and R. A. Brown, Minimization of thermoelastic stresses in Czochralski grown silicon: application of the intergrated system model, *J. Crystal Growth* **108**, 779–805 (1991).
10. C.-C. Hwang, S. Lin and L.-F. Shen, Effects of wall conduction and interface thermal resistance on the phase-change problem, *Int. J. Heat Mass Transfer* **37**, 1849–1855 (1994).
11. C.-C. Hwang and S. Lin, Unsteady thermoelastic analy-

sis of dislocation generation during Czochralski crystal growth, *J. Crystal Growth* **149,** 147–152 (1995).
12. A. Aziz and V. J. Lunardini, Perturbation techniques in phase change heat transfer, *ASME Appl. Mech. Rev.* **46,** 29–66 (1993).
13. A. Aziz, New asymptotic solutions for the variable-property Stefan problem, *Chem. Engng* **16,** 65–68 (1978).
14. R. I. Pedroso and G. A. Domoto, Technical note on planar solidification with fixed wall temperature and variable thermal properties, *ASME J. Heat Transfer* **95,** 553–555 (1973).

APPENDIX

Substituting equations (21)–(24) into equations (11)–(16), we treat them order by order and get the following systems:

For ε^0:

$$\frac{\partial^2\theta_0}{\partial\psi^2} - 2\beta_\tau\theta_0 = 0 \tag{A1}$$

$$\theta_0(\psi, 0) = 1 \tag{A2}$$

$$\theta_0(0, \tau) = 1 \tag{A3}$$

$$\left[\frac{\partial\theta_0}{\partial\psi} + \beta_1\theta_0\right]_{\psi=S} = 0 \tag{A4}$$

$$p_0 = -\left[\frac{\partial\theta_0}{\partial\psi} + \beta_m(\delta - 1)\right]_{\psi=0}. \tag{A5}$$

For ε^1:

$$\frac{\partial^2\theta_1}{\partial\psi^2} - 2\beta_\tau\theta_1 - p_0\left(\frac{\partial\theta_0}{\partial S} + \frac{\partial\theta_0}{\partial\psi}\right) = \begin{cases} -\beta_1^*\dfrac{\partial}{\partial\psi}\left(\theta_0\dfrac{\partial\theta_0}{\partial\psi}\right) & \text{for (I), (II)} \\ 0 & \text{for (III), (IV)} \end{cases} \tag{A6}$$

$$\theta_1(\psi, 0) = 0 \tag{A7}$$

$$\theta_1(0, \tau) = 0 \tag{A8}$$

$$\left[\frac{\partial\theta_1}{\partial\psi} + \beta_1\theta_1\right)_{\psi=S} = \begin{cases} \left[\beta_1^*\theta_0\dfrac{\partial\theta_0}{\partial\psi}\right]_{\psi=S} & \text{for (I), (II)} \\ 0 & \text{for (III), (IV)} \end{cases} \tag{A9}$$

$$p_1 = \begin{cases} -\left[\dfrac{\partial\theta_1}{\partial\psi} + \beta_1^*\theta_0\dfrac{\partial\theta_0}{\partial\psi}\right]_{\psi=0} & \text{for (I), (II)} \\ -\left[\dfrac{\partial\theta_1}{\partial\psi}\right]_{\psi=0} & \text{for (III), (IV)} \end{cases}. \tag{A10}$$

For ε^2:

$$\frac{\partial^2\theta_2}{\partial\psi^2} - 2\beta_\tau\theta_2 - p_0\left(\frac{\partial\theta_1}{\partial S} + \frac{\partial\theta_1}{\partial\psi}\right) - p_1\left(\frac{\partial\theta_0}{\partial S} + \frac{\partial\theta_0}{\partial\psi}\right)$$

$$= \begin{cases} -\dfrac{\partial}{\partial\psi}\left[\beta_1^*\left(\theta_0\dfrac{\partial\theta_1}{\partial\psi} + \theta_1\dfrac{\partial\theta_0}{\partial\psi}\right) + \beta_2^*\theta_0^2\dfrac{\partial\theta_0}{\partial\psi}\right] & \text{for (I)} \\ -\dfrac{\partial}{\partial\psi}\left[\beta_1^*\left(\theta_0\dfrac{\partial\theta_1}{\partial\psi} + \theta_1\dfrac{\partial\theta_0}{\partial\psi}\right) + \beta_2^*\theta_0^2\dfrac{\partial\theta_0}{\partial\psi} + \beta_3^*\theta_0^3\dfrac{\partial\theta_0}{\partial\psi}\right] & \text{for (II)} \\ -\dfrac{\partial}{\partial\psi}\left[\beta_1^*\theta_0\dfrac{\partial\theta_0}{\partial\psi} + \beta_2^*\theta_0^2\dfrac{\partial\theta_0}{\partial\psi}\right] & \text{for (III), (IV)} \end{cases} \tag{A11}$$

$$\theta_2(\psi, 0) = 0 \tag{A12}$$

$$\theta_2(0, \tau) = 0 \tag{A13}$$

$$\left[\frac{\partial\theta_2}{\partial\psi} + \beta_1\theta_2\right]_{\psi=S} = \begin{cases} -\left[\beta_1^*\left(\theta_0\dfrac{\partial\theta_1}{\partial\psi} + \theta_1\dfrac{\partial\theta_0}{\partial\psi}\right) + \beta_2^*\theta_0^2\dfrac{\partial\theta_0}{\partial\psi}\right]_{\psi=S} & \text{for (I)} \\ -\left[\beta_1^*\left(\theta_0\dfrac{\partial\theta_1}{\partial\psi} + \theta_1\dfrac{\partial\theta_0}{\partial\psi}\right) + \beta_2^*\theta_0^2\dfrac{\partial\theta_0}{\partial\psi} + \beta_3^*\theta_0^3\dfrac{\partial\theta_0}{\partial\psi}\right]_{\psi=S} & \text{for (II)} \\ -\left[\beta_1^*\theta_0\dfrac{\partial\theta_0}{\partial\psi} + \beta_2^*\theta_0^2\dfrac{\partial\theta_0}{\partial\psi}\right]_{\psi=S} & \text{for (III), (IV)} \end{cases} \tag{A14}$$

$$p_2 = \begin{cases} -\left[\dfrac{\partial\theta_2}{\partial\psi} + \beta_1^*\left(\theta_0\dfrac{\partial\theta_1}{\partial\psi} + \theta_1\dfrac{\partial\theta_0}{\partial\psi}\right) + \beta_2^*\theta_0^2\dfrac{\partial\theta_0}{\partial\psi}\right]_{\psi=0} & \text{for (I)} \\ -\left[\dfrac{\partial\theta_2}{\partial\psi} + \beta_1^*\left(\theta_0\dfrac{\partial\theta_1}{\partial\psi} + \theta_1\dfrac{\partial\theta_0}{\partial\psi}\right) + \beta_2^*\theta_0^2\dfrac{\partial\theta_0}{\partial\psi} + \beta_3^*\theta_0^3\dfrac{\partial\theta_0}{\partial\psi}\right]_{\psi=0} & \text{for (II)} \\ -\left[\dfrac{\partial\theta_2}{\partial\psi} + \beta_1^*\theta_0\dfrac{\partial\theta_0}{\partial\psi} + \beta_2^*\theta_0^2\dfrac{\partial\theta_0}{\partial\psi}\right]_{\psi=0} & \text{for (III), (IV)} \end{cases} \tag{A15}$$

and

$$A = \sqrt{2\beta_r} \tag{A16}$$

$$B = \beta_1 \tag{A17}$$

$$K = A^2 - B^2 \tag{A18}$$

$$I = (A+B)e^{AS} \tag{A19}$$

$$J = (A-B)e^{-AS} \tag{A20}$$

$$L = I + J \tag{A21}$$

$$C_2 = \frac{p_0(J^2-K)}{2L^2} \tag{A22}$$

$$C_4 = \frac{p_0(I^2-K)}{2L^2} \tag{A23}$$

$$C_5 = \begin{cases} -\dfrac{2\beta_1^* J^2}{3L^2} & \text{for (I), (II)} \\ 0 & \text{for (III), (IV)} \end{cases} \tag{A24}$$

$$C_6 = \begin{cases} -\dfrac{2\beta_1^* I^2}{3L^2} & \text{for (I), (II)} \\ 0 & \text{for (III), (IV)} \end{cases} \tag{A25}$$

$$M = C_2(1+AS+BS)e^{AS} + C_4(1-AS+BS)e^{-AS} + C_5(0.5A+B)e^{2AS} - C_6(0.5A-B)e^{-2AS} \tag{A26}$$

$$N = -(C_5 + C_6) \tag{A27}$$

$$C_1 = \frac{NJ-M}{L} \tag{A28}$$

$$C_3 = \frac{NI+M}{L} \tag{A29}$$

$$F = \begin{cases} \dfrac{A\beta_1^*(I^2-J^2)}{L^2} & \text{for (I), (II)} \\ 0 & \text{for (III), (IV)} \end{cases} \tag{A30}$$

$$G = \begin{cases} -\dfrac{\beta_1^*}{L}[(C_2+C_4)L + 2A(JC_1 - IC_3) + AC_5(I+3J) - AC_6(J+3I)] + \dfrac{A\beta_2^*(I-J)}{L} & \text{for (I)} \\ -\dfrac{\beta_1^*}{L}[(C_2+C_4)L + 2A(JC_1 - IC_3) + AC_5(I+3J) - AC_6(J+3I)] + \dfrac{A\beta_2^*(I-J)}{L} + \dfrac{A\beta_3^*(I^2-J^2)}{L^2} & \text{for (II)} \\ + \dfrac{A\beta_1^*(I^2-J^2)}{L^2} + \dfrac{A\beta_2^*(I-J)}{L} & \text{for (III), (IV)} \end{cases} \tag{A31}$$

$$D_2 = \frac{AK}{L^4}[2A(J^2-K) - p_0L(3J-I)] \tag{A32}$$

$$D_4 = \frac{AK}{L^4}[2A(I^2-K) + p_0L(3I-J)] \tag{A33}$$

$$D_5 = \frac{8\beta_\uparrow^* AKJ}{3L^3} \tag{A34}$$

$$D_6 = -\frac{8\beta_\uparrow^* AKI}{3L^3} \tag{A35}$$

$$X = [(A+B)C_2 + (1+AS+BS)(AC_2+D_2)]e^{AS} - [(A-B)C_4 + (1-AS+BS)(AC_4-D_2)]e^{-AS} + (0.5A+B)(2AC_5+D_5)e^{2AS} + (0.5A-B)(2AC_6)-D_6)e^{-2AS} \tag{A36}$$

$$Y = -(D_5+D_6) \tag{A37}$$

$$D_1 = \frac{L(YJ-ANJ-X)-A(I-J)(NJ-M)}{L^2} \tag{A38}$$

$$D_3 = \frac{L(YI+ANI+X)-A(I-J)(NI+M)}{L^2} \tag{A39}$$

$$E_3 = \frac{p_0(D_2+AC_2)}{4A} \tag{A40}$$

$$E_2 = \begin{cases} \dfrac{1}{2A}\left[p_0(D_1+C_2+AC_1)+\dfrac{Ap_1(LJ-2K)}{L^2}-\dfrac{\beta_\uparrow^* A^2 IC_5}{L}-\dfrac{\beta_2^* A^2 KJ}{L^3}-2E_3\right] & \text{for (I), (II)} \\ \dfrac{1}{2A}\left[p_0(D_1+C_2+AC_1)+\dfrac{Ap_1(LJ-2K)}{L^2}-\dfrac{\beta_2^* A^2 KJ}{L^3}-2E_3\right] & \text{for (III), (IV)} \end{cases} \tag{A41}$$

$$E_6 = -\frac{p_0(D_4-AC_4)}{4A} \tag{A42}$$

$$E_5 = \begin{cases} -\dfrac{1}{2A}\left[p_0(D_3+C_4-AC_3)+\dfrac{Ap_1(LI-2K)}{L^2}-\dfrac{\beta_\uparrow^* A^2 JC_6}{L}-\dfrac{\beta_2^* A^2 KI}{L^3}-2E_6\right] & \text{for (I), (II)} \\ -\dfrac{1}{2A}\left[p_0(D_3+C_4-AC_3)+\dfrac{Ap_1(LI-2K)}{L^2}-\dfrac{\beta_2^* A^2 KI}{L^3}-2E_6\right] & \text{for (III), (IV)} \end{cases} \tag{A43}$$

$$E_8 = \begin{cases} -\dfrac{4\beta_\uparrow^* JC_2}{3L} & \text{for (I), (II)} \\ 0 & \text{for (III), (IV)} \end{cases} \tag{A44}$$

$$E_7 = \begin{cases} \dfrac{1}{3A^2}\left[p_0(D_5+2AC_5)-\dfrac{4\beta_\uparrow^* AJ(C_2+AC_1)}{L}-4AE_8\right] & \text{for (I)} \\ \dfrac{1}{3A^2}\left[p_0(D_5+2AC_5)-\dfrac{4\beta_\uparrow^* AJ(C_2+AC_1)}{L}-4\beta_3^*\dfrac{KA^2J^2}{L^4}-4AE_8\right] & \text{for (II)} \\ -\dfrac{2\beta_\uparrow^* J^2}{3L^2} & \text{for (III), (IV)} \end{cases} \tag{A45}$$

$$E_{10} = \begin{cases} -\dfrac{4\beta_\uparrow^* IC_4}{3L} & \text{for (I), (II)} \\ 0 & \text{for (III), (IV)} \end{cases} \tag{A46}$$

$$E_9 = \begin{cases} \dfrac{1}{3A^2}\left[p_0(D_6-2AC_6)+\dfrac{4\beta_\uparrow^* AI(C_4-AC_3)}{L}+4AE_{10}\right] & \text{for (I)} \\ \dfrac{1}{3A^2}\left[p_0(D_6-2AC_6)+\dfrac{4\beta_\uparrow^* AI(C_4-AC_3)}{L}-4\beta_3^*\dfrac{KA^2I^2}{L^4}+4AE_{10}\right] & \text{for (II)} \\ -\dfrac{2\beta_\uparrow^* I^2}{3L^2} & \text{for (III), (IV)} \end{cases} \tag{A47}$$

$$E^{11} = \begin{cases} -\dfrac{3J}{8L^3}(3\beta_\uparrow^* L^2 C_5+\beta_2^* J^2) & \text{for (I), (II)} \\ -\dfrac{3\beta_2^* J^3}{8L^3} & \text{for (III), (IV)} \end{cases} \tag{A48}$$

$$E_{12}=\begin{cases}-\dfrac{3I}{8L^3}(3\beta_1^*L^2C^6+\beta_2^*I^2) & \text{for (I), (II)}\\ -\dfrac{3\beta_2^*I^3}{8L^3} & \text{for (III), (IV)}\end{cases} \tag{A49}$$

$$E_{13}=\begin{cases}-\beta_3^*\dfrac{4J^4}{15L^4} & \text{for (II)}\\ 0 & \text{for (I), (III), (IV)}\end{cases} \tag{A50}$$

$$E_{14}=\begin{cases}-\beta_3^*\dfrac{4J^4}{15L^4} & \text{for (II)}\\ 0 & \text{for (I), (III), (IV)}\end{cases} \tag{A51}$$

$$V=-(E_7+E_9+E_{11}+E_{12}+E_{13}+E_{14}) \tag{A52}$$

$$E_1=\frac{VJ+U}{L} \tag{A53}$$

$$E_4=\frac{VI+U}{L}. \tag{A54}$$

For (I)

$$\begin{aligned}U=&\left[E_2(1+AS+BS)+E_3S(2+AS+BS)+\frac{\beta_1^*AIC_5}{L}+\frac{\beta_2^*AKJ}{L^3}\right]e^{AS}\\&+\left[E_5(1-AS+BS)+E_6S(2-AS+BS)-\frac{\beta_1^*AJC_6}{L}-\frac{\beta_2^*AKI}{L^3}\right]e^{-AS}\\&+\left[E_8+(2A+B)(E_7+E_8S)+\frac{\beta_1^*J(C_2-2A(C_1+C_2S))}{L}\right]e^{2AS}\\&+\left[E_{10}-(2A-B)(E_9+E_{10}S)+\frac{\beta_1^*I(C_4+2A(C_3+C_4S))}{L}\right]e^{-2AS}\\&+\left[(3A+B)E_{11}+\frac{2\beta_1^*AJC_5}{L}+\frac{\beta_2^*AJ^3}{L^3}\right]e^{3AS}-\left[(3A-B)E_{12}+\frac{3\beta_1^*AIC_6}{L}+\frac{\beta_2^*AI^3}{L^3}\right]e^{-3AS}.\end{aligned} \tag{A55}$$

For (II)

$$\begin{aligned}U=&\left[E_2(1+AS+BS)+E_3S(2+AS+BS)+\frac{\beta_1^*AIC_5}{L}+\frac{\beta_2^*AKJ}{L^3}\right]e^{AS}\\&+\left[E_5(1-AS+BS)+E_6S(2-AS+BS)-\frac{\beta_1^*AJC_6}{L}-\frac{\beta_2^*AKI}{L^3}\right]e^{-AS}\\&+\left[E_8+(2A+B)(E_7+E_8S)+\frac{\beta_1^*J[C_2-2A(C_1+C_2S)]}{L}+\frac{2\beta_3^*AKJ^2}{L^4}\right]e^{2AS}\\&+\left[E_{10}-(2A-B)(E_9+E_{10}S)+\frac{\beta_1^*I[C_4-2A(C_3+C_4S)]}{L}-\frac{2\beta_3^*AKI^2}{L^4}\right]e^{-2AS}\\&+\left[(3A+B)E_{11}+\frac{2\beta_1^*AJC_5}{L}+\frac{\beta_2^*AJ^3}{L^3}\right]e^{3AS}-\left[(3A-B)E_{12}+\frac{3\beta_1^*AIC_6}{L}+\frac{\beta_2^*AI^3}{L^3}\right]e^{-3AS}\\&+\left[(4A+B)E_{13}+\frac{\beta_3^*AJ^4}{L^4}\right]e^{4AS}-\left[(4A-B)E_{13}+\frac{\beta_3^*AI^4}{L^4}\right]e^{-4AS}.\end{aligned} \tag{A56}$$

For (III), (IV)

$$\begin{aligned}U=&\left[E_2(1+AS+BS)+E_3S(2+AS+BS)+\frac{\beta_2^*AKJ}{L^3}\right]e^{AS}+\left[E_5(1-AS+BS)+E_6S(2-AS+BS)-\frac{\beta_2^*AKI}{L^3}\right]e^{-AS}\\&+\left[(2A+B)E_7+\frac{\beta_1^*AJ^2}{L^2}\right]e^{2AS}-\left[(2A-B)E_9+\frac{\beta_1^*AI^2}{L^2}\right]e^{-2AS}+\left[(3A+B)E_{11}+\frac{\beta_2^*AJ^3}{L^3}\right]e^{3AS}-\left[(3A-B)E_{12}+\frac{\beta_2^*AI^3}{L^3}\right]e^{-3AS}.\end{aligned} \tag{A57}$$